J Sol-Gel Sci Technol (2015) 75:625–634
DOI 10.1007/s10971-015-3733-1

ORIGINAL PAPER

Anti-icing performance of transparent and superhydrophobic surface under wind action

Fajun Wang[1,2] · Shan Yu[1] · Junfei Ou[1] · Wen Li[1,2]

Received: 11 January 2015 / Accepted: 2 May 2015 / Published online: 10 May 2015

Abstract In this work, we demonstrated the anti-icing properties of a transparent and superhydrophobic coating surface based on the octadecyltrichlorosilane-modified silica nanoparticles. The surface was prepared via a simple condensation polymerization followed by a spray-coating process. The surface exhibited a high contact angle of 157.5° and a low sliding angle of 6.5° at ambient temperature. The icing behavior of the surface was investigated by successively dropping the 0 °C of water droplets onto the superhydrophobic coating surface at various low temperatures, i.e., –5, –10 and –15 °C with the help of wind action. The surface displayed excellent anti-icing properties at –5 and –10 °C. Water droplets bounced off or slid away the surface before freezing under wind action at the above temperatures. The icing delay time is larger than 2500 s at –10 °C and 5 m/s of wind blow. While at even lower temperature of –15 °C, water froze on the surface quickly. The icing and/or anti-icing mechanisms of the superhydrophobic surface at different temperatures were interpreted by the variation of the surface wettabilities with decreasing temperatures. Specifically, the humidity in air condensed and consequently formed a layer of frost covering the superhydrophobic surface, which has significant influence on the moving abilities of the surface water droplets. As a result, the anti-icing properties of the coating surface changed with the decreasing of temperatures.

Graphical Abstract

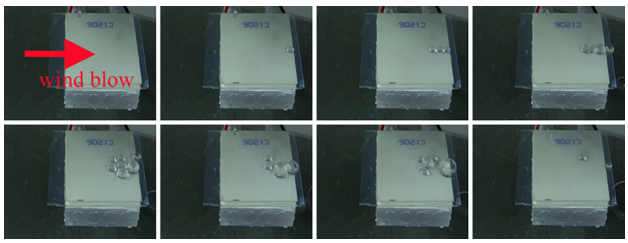

Keywords Transparent · Superhydrophobic surface · Coating · Anti-icing · Silica nanoparticles

1 Introduction

In nature, many surfaces exhibit superhydrophobicity, such as lotus leaf and the wings of butterflies [1–4]. On such surfaces, the contact angle for water is larger than 150° and the roll-off angle is lower than 10° [5, 6]. Various artificial superhydrophobic surfaces have been fabricated by either enhancing the roughness of a hydrophobic surface or modifying a hierarchical structure with low-surface-energy material [7–11]. Superhydrophobic coatings have received much attention over the past decades for their speculated anti-icing and/or icephobic performance and potential applications on aircraft, power lines, insulators, wind turbines and windshields [5, 12–16]. Recent literature survey

Electronic supplementary material The online version of this article (doi:10.1007/s10971-015-3733-1) contains supplementary material, which is available to authorized users.

✉ Fajun Wang
jjbxsjz@foxmail.com

[1] School of Materials Science and Engineering, Nanchang Hangkong University, Nanchang 330063, People's Republic of China

[2] Key Laboratory for Microstructural Control of Metallic Materials of Jiangxi Province, Nanchang Hangkong University, Nanchang 330063, People's Republic of China

indicates the anti-icing and/or icephobic properties of superhydrophobic surfaces were mainly evaluated by the following characteristics. The first is that water (or water droplets) could leave the precooled surface before icing and accumulation [5, 17]. The second is that ice formation on these surfaces could be apparently delayed in comparison with the common surfaces [16–19]. The last is that the ice adhesion between ice layer and the surface is weak and the ice layer could be easily peeled off from the surface [22, 23]. For examples, Cao et al. poured supercooled water at a temperature of –20 °C onto a superhydrophobic-coated Al plate and a pure Al plate (both of the two plates were precooled at –20 °C), respectively. It was observed that ice formed on the pure Al plate immediately upon impinging the surface. While on the superhydrophobic surface, ice formation could not be observed [17]. Zheng et al. prepared a superhydrophobic composite based on ZnO and poly(vinylidene difluoride) (PVDF). Water droplets did not freeze on the surface at a temperature of –20 °C until about 7360 s [18]. Kulinich et al. compared the ice adhesion strength of a superhydrophobic coating on Al alloy plate and a pure polished plate. It was observed that the ice adhesion strength on the superhydrophobic surface was about 5.7 times lower than the pure polished surface of Al alloy [20]. Till now, most of the anti-icing properties were tested under self-designed freezing conditions due to the limitation of standard apparatus for characterizing the performance [12–20]. Other researches studied the icing and/or anti-icing behaviors of superhydrophobic surfaces under natural freezing environment or in a climate-controlled room [17, 22–26]. However, little paper investigating the anti-icing properties under wind action of a transparent and superhydrophobic coating surface has been reported. Compared with the common superhydrophobic coating surfaces, the transparent and superhydrophobic coating surface could be applied in windshields of aircraft for anti-icing because of its transparency. In addition, the actual natural freezing weather conditions often accompanied with wind action, such as the helicopter and fixed wing aircraft in flight and the power lines under rainstorm condition. Most of the icing properties in the literatures were measured under static air conditions, which was different from the actual circumstance. Therefore, it is significant to investigate the anti-icing behavior of a transparent and superhydrophobic coating surface under wind action.

In this work, a transparent and superhydrophobic coating surface based on OTS-modified silica NPs was prepared on glass substrate via a simple spray-coating method. The surface morphology, chemical composition, wettability and transparency were studied. In addition, the icing and anti-icing of the coating surface were tested by successively dropping precooled water droplets onto the cold superhydrophobic surface (precooled at –5, –10 and –15 °C) under wind action. Moreover, the variation of the room-temperature superhydrophobicity of the coating surface with decreasing temperatures was measured and analyzed. Finally, the icing and/or anti-icing behaviors of surfaces with different wettabilities were proposed according to the moving abilities of the water droplets on the surface. It is demonstrated that the coating surface exhibits desirable anti-icing performance at cold temperature of –5 and –10 °C with the help of wind compared with the hydrophobic glass surface.

2 Experimental section

2.1 Materials

Octadecyltrichlorosilane (OTS, 97 %) was obtained from Xiya Chemical Industry Co., Ltd. Ethanol (EtOH, 99.5 %) was purchased from Sinopharm Chemical Reagent Co., Ltd. Silica (SiO_2) nanopaticles (NPs) with average particle size of about 15 nm were purchased from Shanghai Cabot Chemical Corporation. Glass sheet was obtained from the local market.

2.2 Preparation of silica coating

The silica coating was prepared according to the method reported in the literature [27]. Briefly, 2 g of silica nanoparticles was added into 50 mL ethanol and sonicated for about 30 min. Then, 20 μL OTS was carefully added into the dispersion dropwise within 5 s. The dispersion was subjected to magnetic stirring for about 2 h. Finally, a transparent and viscous sol solution was obtained. The sol solution was mixed with ethanol to tune the viscosity of the sol solution (closed to pure water) and then spray-coated onto a clean glass slide or glass sheet using a simple spray bottle [see supporting information (SI, Movie S1)]. After coating, the sample was dried at 140 °C for 2 h and naturally cooled to the ambient temperature. It should be mentioned that the simple spray-coating method could be applied on various surfaces with large size and complex shape.

2.3 Characteristics

The water contact angle (CA) and water sliding angle (SA) were measured using a Krüss DSA 100 apparatus (Germany) with 4 μL of water droplet according to the reported method [13]. The shape and aggregation state of silica NPs were examined by transmission electron microscopy (TEM, FEI Tecnai G20, USA). The surface microstructure of the superhydrophobic coating was measured with a

field-emission scanning electron microscopy (FESEM, NanoSEM-450, FEI-Nova, America). The surface asperity was measured using an atomic force microscope (AFM, D3000, Veeco, Inc., USA). The light transmittance was measured using an ultraviolet and visible spectrophotometer (UV-3100PC, Shimadzu, Japan). The icing performance of the sample was measured using a homemade apparatus as depicted in Fig. 1a. The temperature of the thermoelectric cooler (top surface) could be tuned from room temperature to –24 °C. For the icing performance measurement, the temperature of the cooler was precooled to a certain temperature (i.e., –5, –10, –15 °C). Then, a sheet of sample was placed onto the surface of the cooler to precool the sample surface. Afterward, water droplets (precooled, temperature = 0 °C, volume = ~8 μL) were successively dropped onto the sample surface from a height of 3 cm at a speed of 2 drops per second (see SI, Movie S2). All the icing-behavior measurement was taken under predetermined conditions, i.e., temperature of 0 ± 2.5 °C and RH of 35 ± 6.7 %. Particularly, wind action (with a speed of 0 m/s, 1 m/s, 3 m/s and 5 m/s, respectively) was generated using an electric fan to help the movement of water droplets on the cold surface of the sample (see Fig. 1b). The process of water droplets continuously impinging onto the sample surface was recorded with a camera.

3 Results and discussion

The TEM image of the as-received silica NPs was shown in Fig. 2a. One can see that the silica NPs show spherical shape with particle size ranging from 12 to 30 nm. In addition, the silica NPs were stringed together and formed aggregates. Figure 2b shows the schematic illustration of the aggregate structures of silica NPs with various shapes and sizes [6, 27–29]. In addition, the surface of silica NPs is full of hydroxyl groups [27–29]. Figure 3a shows the hydrolysis and condensation reactions of OTS with adsorbed moistures (i.e., H_2O from air) in ethanol solution. During the condensation reactions, polyhydroxy polysiloxane with different molecular weight and structure are formed (different n, Fig. 3a) [5, 27, 28]. The reactions between the hydroxyl groups of the silica NPs and the polysiloxane could also occurred (Fig. 3b, c, e). As a result, even larger aggregate of silica NPs is formed (Fig. 3c). After spray-coated on glass substrate and then dried, superhydrophobic coating surface was obtained (Fig. 3d). Importantly, the coating and the glass substrate are also chemical bound (Fig. 3f). The superhydrophobic coating was immersed in ethanol under ultrasonication (120 W, 40 kHz and 60 °C) for 30 min. It was found that the coating keeps its superhydrophobicity (CA > 150° and SA < 10°) after ultrasonic treatment, which demonstrated the stability of the coating.

The surface wettabilities of the superhydrophobic coating on glass slide and the pure glass slide are shown in Fig. 4. The pure glass is hydrophilic. Water droplet exhibits CA of 42.7 ± 3.2° on the pure glass surface (Fig. 4a) and without sliding even when the surface is tilted at 90°. In addition, CA 157.5 ± 2.3° and SA 6.5 ± 1.7° for water droplet are observed on the coating surface, showing its superhydrophobicity (Fig. 4b). In addition, Fig. 4 also shows the transparency of the superhydrophobic coating. The superhydrophobic coating is optically transparent, as can be seen in Fig. 4a. The words on the typing paper could be clearly observed through the glass slide and the superhydrophobic coating. The transmittance of the glass substrate and the coating are shown in Fig. 4c. One can see that the transmittance of the coating is slightly lower than the bare glass in low wavelength range (380–550 nm) and slightly higher than the bare glass in high wavelength range (550–790 nm) [27]. However, the transmittance of the

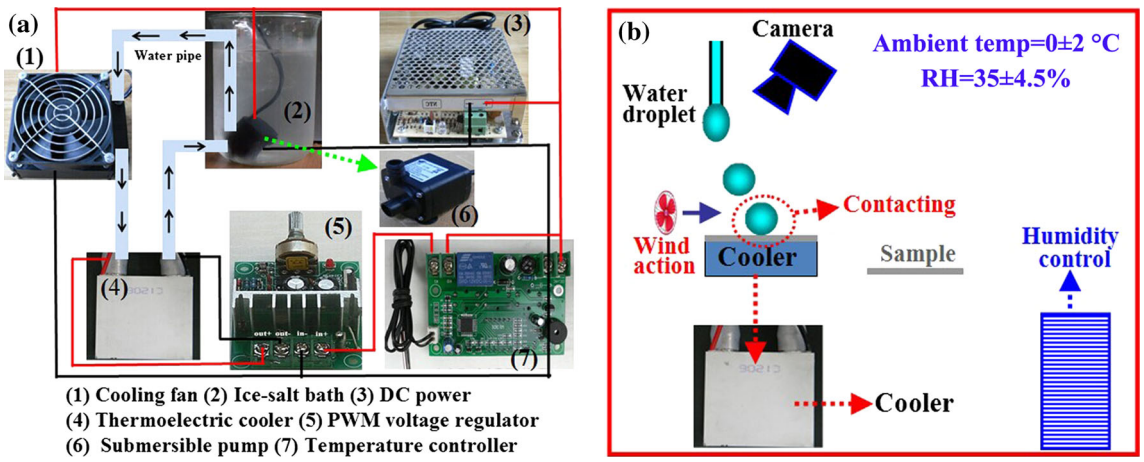

Fig. 1 **a** The composition of the homemade icing-behavior measuring apparatus and **b** the schematic illustration of the measuring method

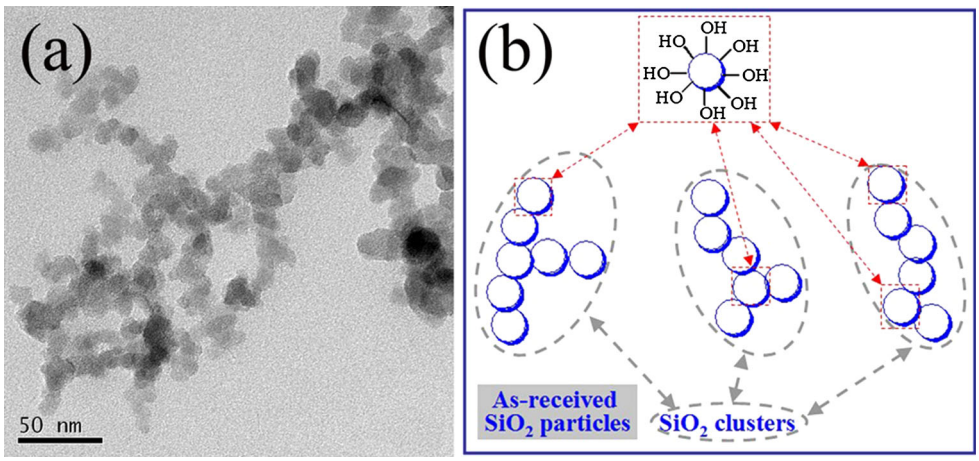

Fig. 2 **a** TEM image of the as-received silica NPs. **b** Schematic illustration for the aggregate structures of the silica NPs and the surface chemical hydroxyl group

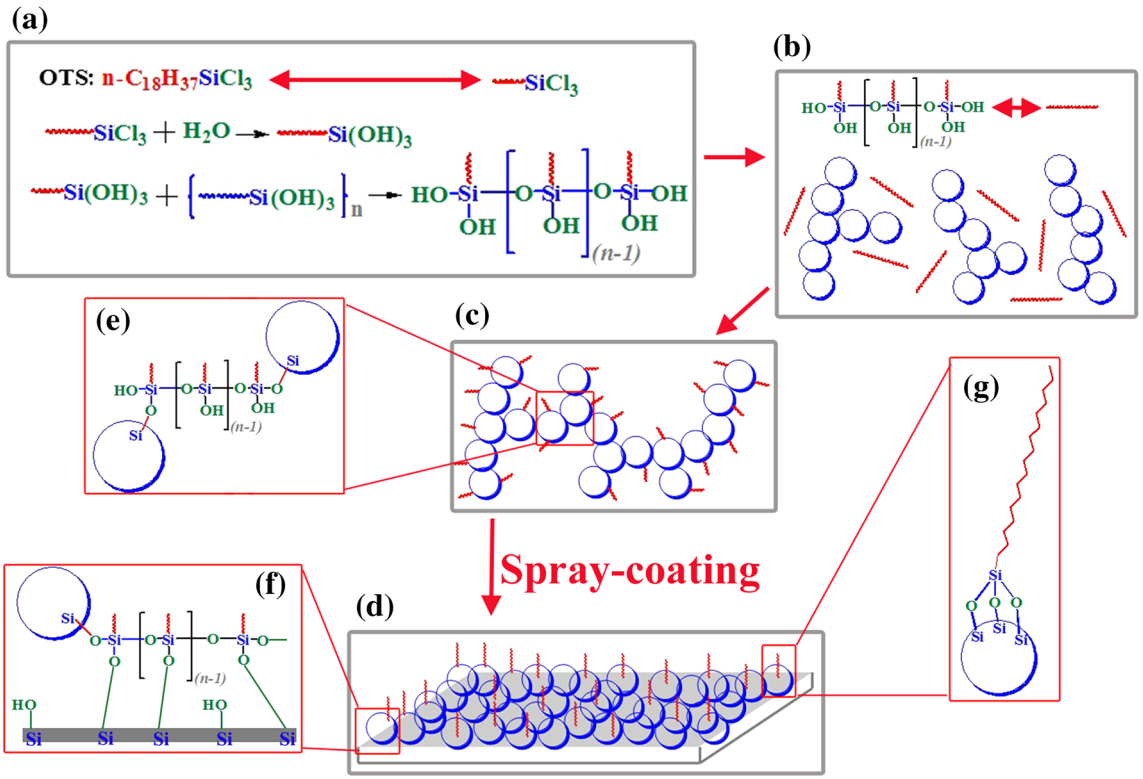

Fig. 3 Schematic illustrations of synthesis silica sol solution and the preparation of silica coating by spray coating. **a** The hydrolysis and condensation reactions between OTS and adsorbed water in ethanol; **b** the as-received silica NPs and the hydrolysis and condensation products of OTS; **c** the structure of sol; **d** the structure of silica coating on glass substrate; **e** the chemical bond between two silica NP aggregates; **f** the chemical bond between the coating and the glass substrate; **g** the surface chemical composition of the silica coating

superhydrophobic coating is always larger than 81.5 % in the whole wavelength range of visible light (380–790 nm).

It was generally believed that the superhydrophobicity of a surface was determined by two factors, i.e., surface roughness and surface chemical composition. The artificial superhydrophobic surfaces were usually prepared by two methods [1, 7, 8]. One is creating micro- and/or nanostructures on intrinsically hydrophobic surface [27]. The other is modifying a rough surface with low-surface-energy material [28]. Hence, the surface morphology, topography (asperity) and chemical composition were investigated. Figure 5a shows the FESEM image of the superhydrophobic coating. Silica NPs form large amount of dense and continuous aggregates covering the surface of glass slide. The typical sizes of the randomly dispersed silica NPs were mainly in the range of 50–200 nm. In addition, a

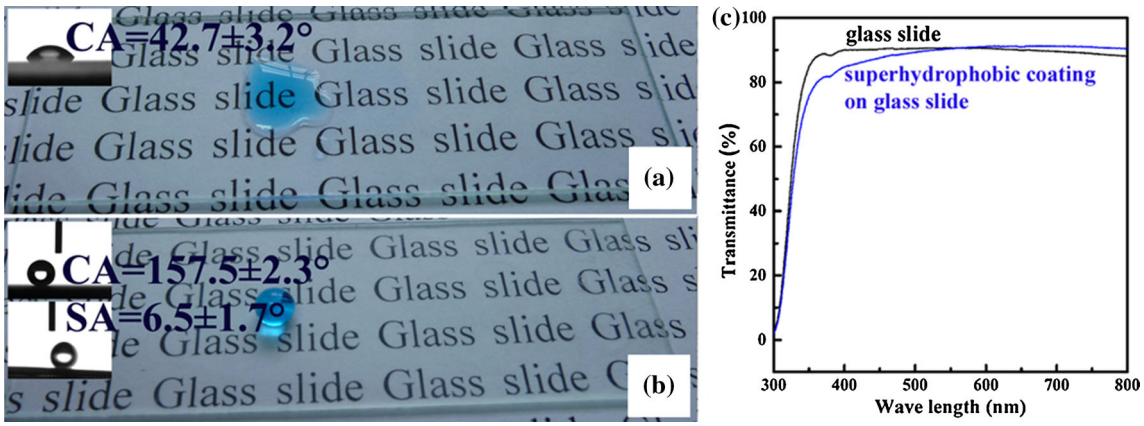

Fig. 4 Digital pictures of water droplet (dyed with color) on different sample surface. **a** The bare glass slide; **b** the superhydrophobic coating on glass slide; **c** UV–Vis transmittance of glass slide and the superhydrophobic coating on glass slide. The *insets* show the measurement of CA and SA

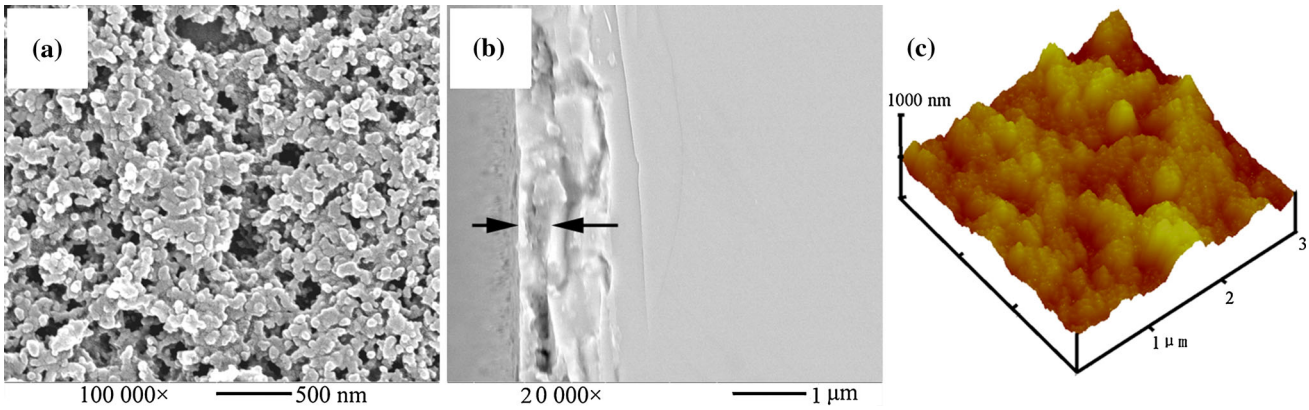

Fig. 5 **a** FESEM image of the superhydrophobic coating; **b** a cross section of the FEM image; **c** corresponding AFM image of the superhydrophobic coating

large number of micropores were also revealed in the FESEM image. The thickness of the coating on the glass substrate is about 400–600 nm (Fig. 5b). The AFM analysis of the coating surface was shown in Fig. 5c. The results indicated that the root-mean-square roughness (R_r) of the surface is 64.7 nm, the mean roughness (R_a) is 51.7 nm and the roughness factor is 1.42, respectively [6, 27–29]. Hence, the roughness of the coating is much lower than the wavelength of visible light (380–790 nm), which could interpret the transparence of the superhydrophobic coating [6, 32]. The XPS spectrum reveals the existence of the element of C, O and Si (Fig. 6a) [33, 34]. The element of C is assigned to the modification of OTS on the coating surface. The elements of O and Si are attributed to the O and Si of silica NPs and the chemical bound OTS. The high-resolution XPS spectra of the sample at C 1 s, O 1 s and Si 2p region were also measured and are shown in Fig. 6b–d, respectively. C1 s peak centered at bind energy of 284.7 eV, O 1 s peak at 532.7 eV and Si 2p at 103.6 eV were detected by XPS, indicating the existence of OTS on the sample surface. Therefore, the rough microstructures of the coating surface combined with the surface chemical bound low-surface-energy OTS are responsible for the superhydrophobicity of the coating.

The icing and anti-icing behaviors of the superhydrophobic-coated glass substrate at a temperature of –10 °C were investigated and depicted in Fig. 7. The freeze of water droplet on the cold surface can be judged by the shape and the movement of water droplet on the surface. As can be seen in Fig. 7a1–h1, water droplets were adsorbed and gradually accumulated on the superhydrophobic surface without the help of wind. The spread water will freeze quickly due to the low surface temperature (–10 °C) and the large contact area (see Fig. 7h1). Movie S2 shows the icing and/or anti-icing behaviors of the superhydrophobic coating surface at different temperatures, i.e., –5, –10 and –15 °C. As can be seen from Movie S2(a), the coating surface at –5 °C is still

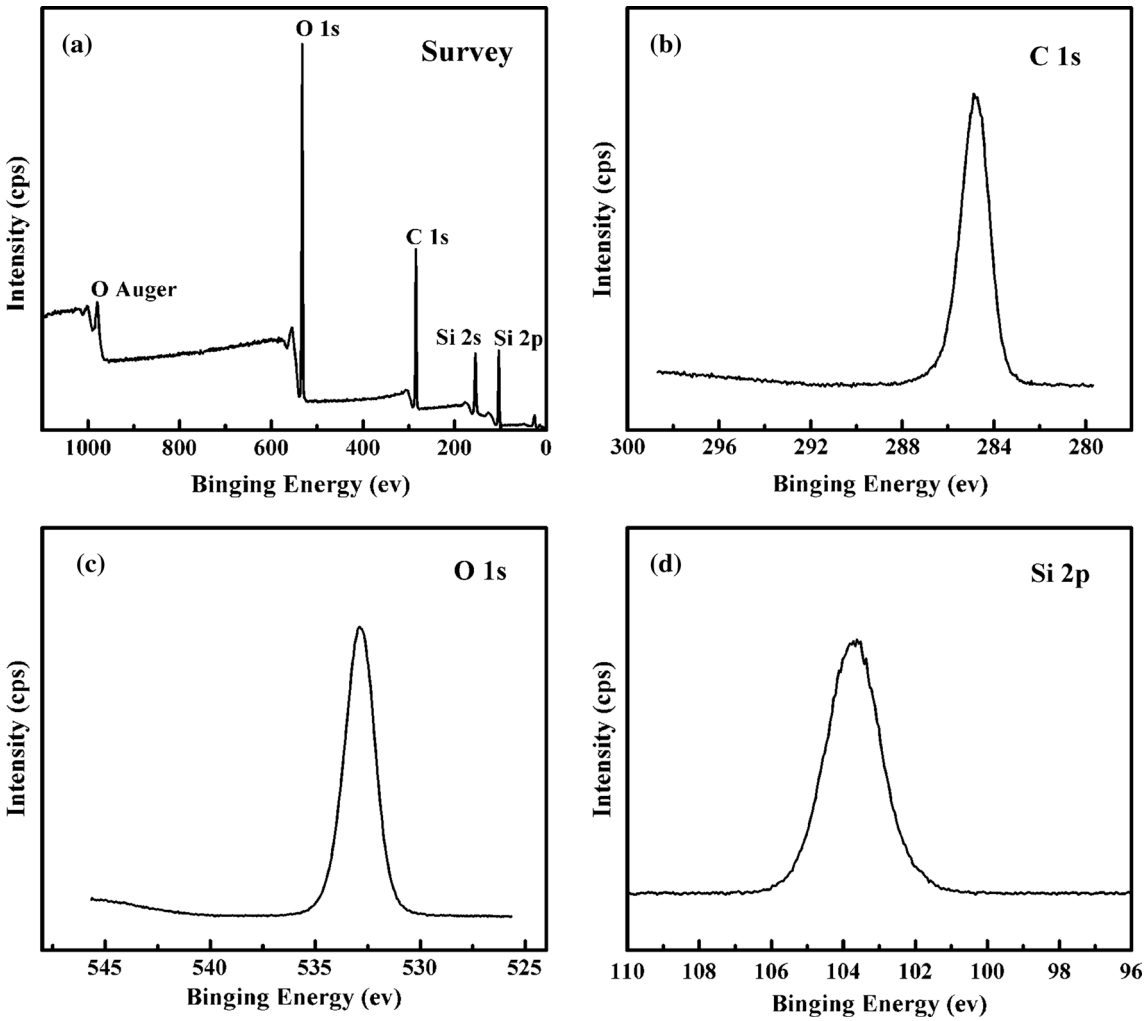

Fig. 6 XPS spectrum of the superhydrophobic coating. **a** Survey spectrum; high-resolution spectra of **b** C 1 s region; **c** O 1 s region; **d** Si 2p region

superhydrophobic. Water droplet bounced off the surface as soon as it impinged on the surface. After successively adding water droplets onto the coating surface for about 30 min, the surface was still clean, without any water and/or ice remained on it. However, the superhydrophobicity of the coating surface could be changed at a lower temperature of –10 °C, as can be seen in Movie S2(b). Water droplets exhibited large CA on the surface but could not slide immediately away the surface under wind action. However, with continuously adding of water droplets, the droplets merged together and formed larger droplets. Consequently, the large droplets slid away the surface successfully with the help of wind (also see Fig. 7a2–h2). Importantly, water droplets showed apparent CA lower than 150° could be observed by naked eyes (Fig. 7b1, c1, b2, cannot roll off), which revealed that the room-temperature superhydrophobicity of the coating surface was changed at the temperature of –10 °C. However, the surface water droplets could roll away the surface readily under wind action (Fig. 6a2–h2). In addition, ice formation on the coating surface could also not be observed even after 30 min, which demonstrated the icing delay performance. At even lower temperature of –15 °C, water droplet with an apparent CA lower than 90° always adhered to the coating surface firmly without sliding under wind blow [Movie S2(c)]. As a result, water froze quickly on the coating surface.

The variation of CA of the coating surface with temperature was carefully investigated using the CA measuring apparatus, and the results are shown in Fig. 8. Water droplet on the coating surface at the temperatures of –5, –10 and –15 °C exhibited a CA of 158.8 ± 2.3°, 127.3 ± 3.1° and 79.5 ± 2.8°, respectively. The variation of CA could be interpreted by the formation of condensed water and frost on the coating surface [5, 13, 35, 36]. In the present case, the coating surface was at temperatures significantly lower than 0 °C, while the ambient temperature

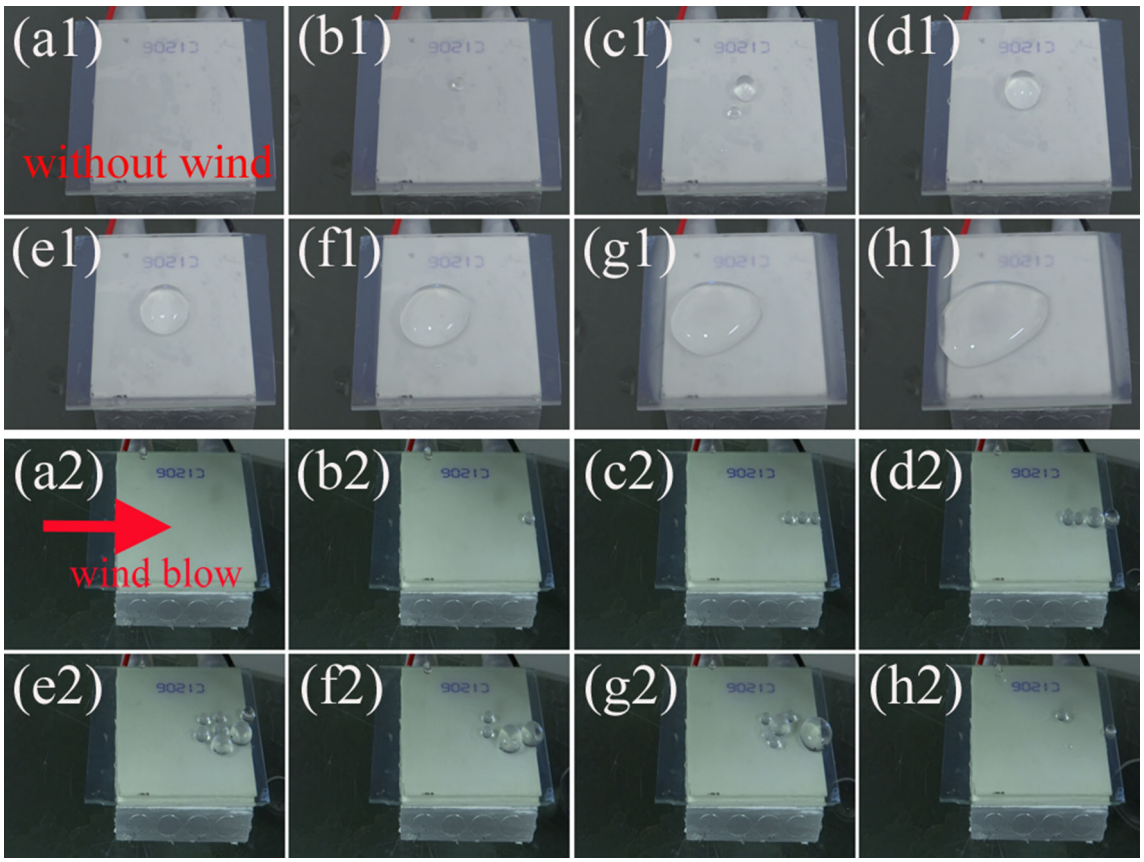

Fig. 7 Icing and anti-icing processes of superhydrophobic sample at –10 °C. **a1–h1** without wind blow; **a2–h2** under wind blow

was about 0 °C. As we know, water vapor in air could condense and consequently form frost on the coating surface [13, 18]. Figure 8a shows the magnified image recorded by the CA measuring apparatus (optical microscope) at a temperature of –5 °C. Condensed small water droplets could be observed on the surface. However, the condensed small droplets could be merged by the impinging droplets and then slid away the surface under wind action. At lower temperature of –10 °C, the condensed small droplets could not be observed, while a layer of frost was appeared on the coating surface. The impinging warm water droplet melted the cold frost partially upon contacting and adsorbed by the adjacent frost. As a result, CA reduced to 127.3 ± 3.1° (Fig. 8b). At even lower temperature of –15 °C, the frost formed on the coating surface was denser and the temperature was much lower, as shown in Fig. 8c. The impinging water droplet could not melt the frost effectively, but froze on the frost surface upon the interchange of heat. Therefore, the CA further decreased to 79.5 ± 2.8° on the coating surface at the temperature of –15 °C. In addition, the contact area increased apparently with the decreasing of temperature (see Fig. 8a–c). Both the increasing of contact area and the decreasing of temperature resulted in the decrease of freezing time of water droplet on the surface (i.e., delay ice formation).

Figure 9 shows the icing delay time of water droplet on the superhydrophobic coating surface at different temperatures and various wind velocities (i.e., 0, 1, 3 and 5 m/s). It is observed that the delay time depends on both temperature and wind velocity. As can be seen in Fig. 9, at the measuring temperature of –5 and –15 °C, the delay time is about 522 and 2 s, respectively, which is nearly constant with decreasing temperature. However, at the measuring temperature of –10 °C, the delay time increases sharply with the increase of wind velocity. The delay time achieves above 2500 s at a wind velocity of 5 m/s. The significant increase of delay time with the increase of temperature can be interpreted by two factors: Firstly, the ambient temperature (0 °C) is higher than the sample (–10 °C). Therefore, the wind is warm and can increase the temperature of the water droplet. The higher the wind velocity is, the warmer the water droplet is. Secondly, the water droplet can slide on the sample surface with the help of wind, which can decrease the contact time between water droplet and the surface. The results revealed that the superhydrophobic surface could delay ice formation on its surface due to the low contact area and/or low contact time

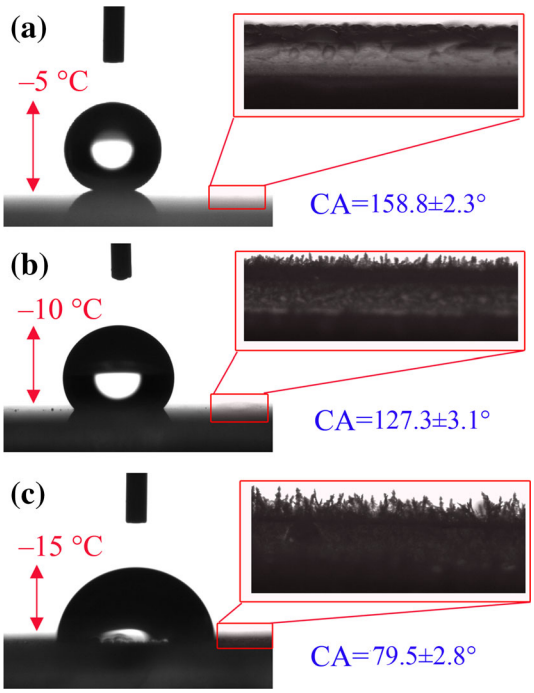

Fig. 8 CA measurement of the coating surface at different temperatures and the corresponding optical image of the condensed water and/or frost formed on the coating surface. **a** At –5 °C; **b** at –10 °C; and **c** at –15 °C

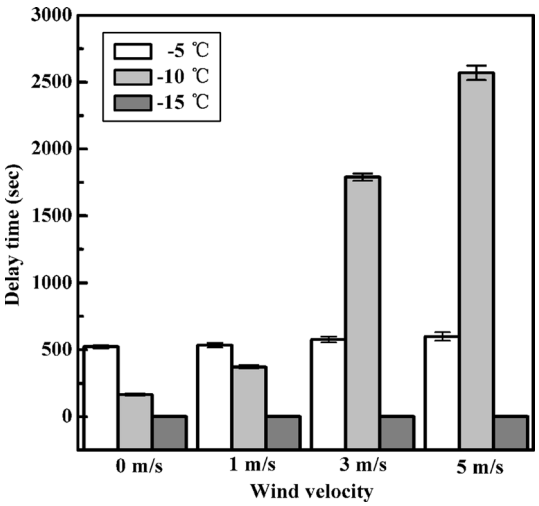

Fig. 9 Freezing delay time of water droplet on the superhydrophobic coating surface at different temperatures and wind velocities

(see Fig. 9a, b). However, at even lower temperature of –15 °C, the water droplet spreads on the sample surface and cannot move even with the help of wind, which results in larger contact area and longer contact time. Therefore, the water droplet freezes quickly.

The variation of CA on a solid surface with temperature could be used to interpret the icing and/or anti-icing properties of a solid surface. Figure 10 shows the icing and anti-icing mechanisms of samples with different surface wettabilities under wind action. As we all know, solid surfaces are divided into three types according to the surface CA for water, i.e., hydrophilic surface (CA < 90°), hydrophobic surface (90° < CA < 150) and superhydrophobic surface (CA > 150°) [2]. When water droplet makes contact with a hydrophilic surface, both the contact area and the adhesion strength are high. As a result, surface water cannot move away easily even under wind action and finally froze on the hydrophilic surface (Fig. 10a, b) [18]. On the contrary, when the cold surface is superhydrophobic at the temperature of –5 °C, i.e., CA > 150° and SA < 10°, both the contact area and the adhesion force are small; thus, water droplet is easy to roll away under wind blow, or even bounced off the surface spontaneously without the help of wind action [37, 38]. Hence, water droplets have little chances to ice up, and the surface is anti-icing (Fig. 10c). At temperature of –10 °C, the coating surface is hydrophobic due to the formation of a layer of frost (Figs. 8b, 10d). Water droplet sticks to the coating surface and cannot roll away spontaneously. However, with the help of wind, water droplet slid slowly and finally left the surface before freezing (Fig. 10d). At a much lower temperature of –15 °C, the coating surface is hydrophilic due to the dense frost on the coating surface (Fig. 8c). Hence, the adhesion force between the droplet and the surface is much stronger. As a result, water droplets continuously accumulated on the coating surface without moving even under wind action and consequently froze on the coating surface (Fig. 10f).

4 Conclusion

A transparent and superhydrophobic coating surface was fabricated based on OTS-modified SiO_2 particles via a simple spray-coating method. The coating surface exhibits a transmittance above 81.5 % in the whole wavelength range of visible light (i.e., 380–790 nm), high CA of 157.5° and low SA of 6.5° simultaneously. In addition, water droplets were successively dropped onto the precooled coating surface (–5, –10 and –15 °C) under wind action to evaluate the anti-icing properties of the coating. It was revealed that the coating surface exhibited anti-icing properties at the temperatures of –5 and –10 °C. Water droplets bounced off the surface quickly at –5 °C and slid away the surface at –10 °C with the help of wind. Ice formation could be delayed on such surface for more than 2500 s at the measuring temperature of –10 °C and a wind velocity of 5 m/s. However, at even lower temperature of –15 °C, water accumulated and iced up on the coating surface quickly. Furthermore, the icing and anti-icing mechanisms of samples with different surface wettabilities

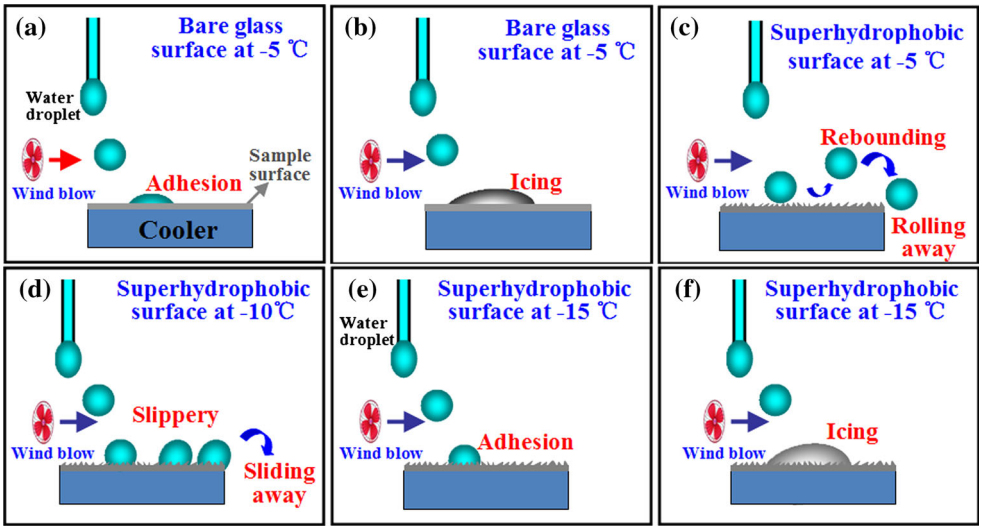

Fig. 10 Icing and anti-icing mechanisms of samples with different surface wettabilities at different temperatures under wind action. **a**, **b** Hydrophilic surface of glass substrate at –5 °C; **d** room-temperature superhydrophobic surface at different temperatures: **d** at –5 °C; **e** at –10 °C; and **f–h** at –15 °C

under wind action were proposed. It was suggested that the condensed water and a layer of frost formed on the coating surface played an important role in determining the icing and/or anti-icing properties of the coating surface. Therefore, the transparent and superhydrophobic coating surface could be applied on the windshields of aircrafts and automobiles for self-clean and anti-icing application.

Acknowledgments The authors acknowledge the financial support by the National Natural Science Foundation of China (Grant No. 51263018), International S&T Cooperation Program of China (Grant No. 2012DFA51200), Science and Technology Supporting Plan of Jiangxi Province, Social Development Field (Grant Nos. 20122BBG70165) and Industrial Field (20133BBE50007), and the Key Laboratory for Microstructural Control of Metallic Materials of Jiangxi Province (Grant No. JW201423002).

References

1. Bhushan B, Jung YC (2011) Prog Mater Sci 56:1–108
2. Ganesh VA, Raut HK, Nair AS, Ramakrishna SJ (2011) Mater Chem 21:16304–16322
3. Sun TL, Qing GY, Su BL, Jiang L (2011) Chem Soc Rev 40:2909–2921
4. Neinhuis C, Koch K, Barthlott W (2011) Planta 213:427–434
5. Wang YY, Xue J, Wang QJ, Chen QM, Ding JF (2013) ACS Appl Mater Interfaces 5:3370–3381
6. Wen XF, Wang K, Pi PH, Yang JX, Cai ZQ, Zhang LJ, Qian Y, Yang ZR, Zheng DF, Cheng J (2011) Appl Surf Sci 258:991–998
7. Davis A, Yeong YH, Steele A, Bayer IS, Loth E (2014) ACS Appl Mater Interfaces 6:9272–9279
8. Bahadur V, Mishchenko L, Hatton B, Taylor JA, Aizenberg J, Krupenkin T (2011) Langmuir 27:14143–14150
9. Jin CF, Yan RS, Huang JG (2011) J Mater Chem 21:17519–17525
10. Jin CF, Jiang YF, Niu T, Huang JG (2012) J Mater Chem 22:12562–12576
11. Li SJ, Wei YQ, Huang JG (2010) Chem Lett 39:20–21
12. Mishchenko L, Hatton B, Bahadur V, Taylor JA, Krupenkin T, Aizenberg J (2010) ACS Nano 4:7699–7707
13. Guo P, Wen MX, Wang L, Zheng YM (2014) Nanoscale 6:3917–3920
14. Oberli L, Caruso D, Hall C, Fabretto M, Murphy PJ, Evans DC (2014) Adv Colloid Interface Sci 210:47–57
15. Lee YW, Yu KY, Lee JK (2010) Langmuir 26:14110–14130
16. Wang FJ, Lei S, Xue MS, Ou JF, Li CQ, Li W (2014) J Phys Chem C 118:6344–6351
17. Cao LL, Jones AK, Sikka VK, Wu JZ, Gao D (2009) Langmuir 25:12444–12448
18. Wen MX, Lei L, Zhang MQ, Jiang L, Zheng YM (2014) ACS Appl. Mater. Interfaces 6:3963–3968
19. Yang J, Li W (2013) J Alloy Compd 576:215–219
20. Zhang YF, Yu XQ, Wu H, Wu J (2012) Appl Surf Sci 2012(258):8253–8257
21. Boinovich L, Emelyanenko AM, Korolev VV, Pashinin AS (2014) Langmuir 30:1659–1668
22. Kulinich SA, Farzaneh M (2011) Cold Reg Sci Technol 65:60–64
23. Kulinich SA, Farzaneh M (2009) Appl Surf Sci 255:8153–8157
24. Li XY, Yang BB, Zhang YQ, Gu GT, Li MM, Mao LQ (2014) J Sol-Gel Sci Technol 69:441–447
25. Zhang ZJ, Jiang XH, Sun CX, Hu JL, Huang HZ (2012) IEEE Trans Dielectr Electr Insul 19:1070–9878
26. Tarquini S, Antonini C, Amirfazli A, Marengo M, Palacios J (2014) Cold Reg Sci Technol 100:50–58
27. Li J, Wan HQ, Ye YP, Zhou HD, Chen JM (2012) Appl Surf Sci 261:470–472
28. Wang SD, Luo SS (2012) Appl Surf Sci 258:5443–5450
29. Mahadik SA, Mahadik DB, Kavale MS, Parale VG, Wagh PB, Barshilia HC, Gupta SC, Hegde ND, Rao AV (2012) J Sol-Gel Sci Technol 63:580–586
30. Hou WX, Wang QH (2009) J Colloid Interf Sci 333:400–403
31. Isimjan TT, Wang TY, Rohani S (2012) Chem Eng J 210:182–187
32. Xu L, Karunakaran RG, Guo J, Yang S (2012) ACS Appl Mater Interfaces 4:1118–1125
33. Yang H, Zhang XJ, Cai ZQ, Pi PH, Zheng DF, Wen XF, Cheng J, Yang ZR (2011) Surf Coat Tech 205:5387–5393
34. Yang HW, Cheng YR, Xiao F (2011) Appl Surf Sci 258:1572–1580

35. Rykaczewski K, Anand S, Subramanyam SB, Varanasi KK (2013) Langmuir 29:5230–5238
36. Kulinich SA, Farhadi S, Nose K, Du XW (2011) Langmuir 27:25–29
37. Feng J, Qin ZQ, Yao SH (2012) Langmuir 28:6067–6075
38. Boreyko JB, Chen CH (2009) Phys Rev Lett 103:184501-1–184501-4